CHINESE OPTICS LETTERS

Vol. 21, No. 10 | October 2023

Controlled generation of order-switchable cylindrical vector beams from a Nd:YAG laser

Longyang Cao (曹龙阳)[1], Mingming Zhang (张明明)[1], Jiantai Dou (窦健泰)[1], Jiang Zhao (赵 江)[2], Youyou Hu (胡友友)[1*], and Bo Li (李 波)[3**]

[1] Department of Optoelectronic Information of Science and Engineering, School of Science, Jiangsu University of Science and Technology, Zhenjiang 212100, China

[2] Key Laboratory of Ferro and Piezoelectric Materials and Devices of Hubei Province, Faculty of Physics and Electronic Science, Hubei University, Wuhan 430062, China

[3] School of Optical and Electronic Information, Huazhong University of Science and Technology, Wuhan 430074, China

*Corresponding author: yyhu@just.edu.cn

**Corresponding author: libohust@hust.edu.cn

Received December 26, 2022 | Accepted May 5, 2023 | Posted Online August 21, 2023

We reporte and demonstrate a solid-state laser to achieve controlled generation of order-switchable cylindrical vector beams (CVBs). In the cavity, a group of vortex wave plates (VWPs) with two quarter-wave plates between the VWPs was utilized to achieve mode conversion and order-switch of CVBs. By utilizing two VWPs of first and third orders, the second and fourth order CVBs were obtained, with mode purities of 96.8% and 94.8%, and sloping efficiencies of 4.45% and 3.06%, respectively. Furthermore, by applying three VWPs of first, second, and third orders, the mode-switchable Gaussian beam, second, fourth, and sixth order CVBs were generated.

Keywords: cylindrical vector beams; order-switchable beams; vortex wave plates; solid-state laser.
DOI: 10.3788/COL202321.101401

1. Introduction

In recent years, cylindrical vector beams (CVBs) have attracted much attention because of their unique features from the cylindrically symmetric electric field[1]. Different from linearly or circularly polarized beams with a uniform polarization state, the intensity of CVBs at the optical axis is zero[2], which gives rise to many applications, such as optical communication[3], optical trapping[4], and optical storage[5]. Compared with low-order CVBs, the azimuthal modes of high-order CVBs have more than one rotation of the polarization vector, whereas their radial modes have a few radial nodes in the electric field[6]. So, high-order CVBs have been demonstrated for potential applications in high-capacity storage[7], information processing[8], quantum entanglement[9], high-resolution imaging[10], optical trapping[11], and optical communication[12]. Particularly, the higher-order CVBs can scale the transmission capacity in optical communication[12].

So far, many methods have been developed to generate high-order CVBs[13–17], which are mainly divided into two methods: the extracavity method[18] and the intracavity method[19]. The extracavity method refers to the conversion of Gaussian beams into high-order CVBs outside the resonator by applying spatial light modulators (SLMs)[20], subwavelength dielectric gratings[21], q-plates[22–24], digital micromirror devices (DMDs)[25], birefringence elements[26], and so on[27,28]. However, in the process of beam shaping, the energy conversion efficiency of the extracavity method is lower than that of the intracavity method due to the loss caused by diffraction loss; other reasons exist in the extracavity method, and the beam quality of the extracavity method is not very high. In contrast, the intracavity method can directly generate high-order CVBs in laser resonators[19,29], which have higher energy conversion efficiency and better beam quality[30,31]. In recent years, many attempts have been made to generate these modes in laser cavities based on the thermal lens effect[29], q-plates[32–36], digitally addressed holography[36], and so on. Among them, the q-plate or so-called vortex wave plate (VWP)[37] has been utilized to directly generate high-order CVBs in solid-state laser and fiber laser due to its variability and accessibility[19,32–35]. However, these lasers can only achieve the mode-switch of high-order CVBs in a unique order. To the best of our knowledge, there have been no reports about the controlled generation of mode-switchable high-order CVBs between different orders in a solid-state laser.

In this Letter, we report and demonstrate a compact solid-state laser to obtain controlled generation of mode-switchable

higher-order CVBs between different orders. In the cavity, a group of VWPs with two cascaded quarter-wave plates (QWPs) between the VWPs were utilized to achieve the mode conversion between linearly polarized TEM_{00} mode and CVBs, as well as the mode-switch of CVBs between different orders. Based on the Jones matrix theory, we verified that by manipulating the orientation of the two QWPs, the addition and subtraction of the orders of VWPs can be achieved, which becomes an order-switchable VWP (OSVWP). Then, a solid-state laser was built to obtain controlled generation of mode-switchable higher-order CVBs between different orders. By applying two or three VWPs with the order of m_1, m_2, or m_1, m_2, m_3, mode-switchable CVBs of order $m = m_2 \pm m_1$ or $m = m_3 \pm m_2 \pm m_1$ were achieved.

2. Methods

The VWP can be seen as a spatially variant half-wave plate (HWP), of which the fast axis rotates continuously around a singularity point. It can convert linearly or circularly polarized beams into CVBs or vortex beams with a transmission efficiency of 96%. The orientation of its fast axis can be expressed as

$$\theta(\varphi) = \frac{m}{2}\varphi + \varphi_0, \tag{1}$$

where θ is the fast axis direction of the given azimuth angle φ on the wave plate, φ_0 is the orientation of fast axis at $\varphi = 0$, and m is the order of the VWP. For convenience, let $\varphi_0 = 0$, and the Jones matrix of VWP can be written as

$$J_{\mathrm{VWP}}(\theta) = \begin{bmatrix} \cos 2\theta & \sin 2\theta \\ \sin 2\theta & -\cos 2\theta \end{bmatrix}. \tag{2}$$

In addition, the Jones matrices of the HWP and QWP are

$$J_{\mathrm{HWP}}(\alpha) = \begin{bmatrix} \cos 2\alpha & \sin 2\alpha \\ \sin 2\alpha & -\cos 2\alpha \end{bmatrix}, \tag{3}$$

$$J_{\mathrm{QWP}}(\beta) = \begin{bmatrix} 1 - i\cos 2\beta & -i\sin 2\beta \\ -i\sin 2\beta & 1 + i\cos 2\beta \end{bmatrix}, \tag{4}$$

where α and β are the angles between the fast axis and the 0° axis of the HWP and QWP, respectively. Due to the limited order availability of VWPs, a new VWP can be implemented by cascading two or more VWPs together,

$$J_2 \cdot J_1 = J_{m_2} \cdot J_{m_1} = \begin{bmatrix} \cos(m_2 - m_1)\varphi & \sin(m_2 - m_1)\varphi \\ \sin(m_2 - m_1)\varphi & -\cos(m_2 - m_1)\varphi \end{bmatrix} = J_{m_2 - m_1}. \tag{5}$$

It is found that a VWP of $(m_2 - m_1)^{\mathrm{th}}$ order can be realized. When the HWP is inserted into two cascaded VWPs[22], the VWP of $(m_2 + m_1)^{\mathrm{th}}$ order is formed,

$$J_2 \cdot J_{\mathrm{HWP}} \cdot J_1 = J_{m_2} \cdot J_{H_x} \cdot J_{m_1} = J_{m_2 + m_1}, \tag{6}$$

where H_x represents the fast axis of the HWP along the x axis. So, we can realize the addition and subtraction of the order of VWPs by applying two QWPs between them, as shown below,

$$J_{m_2 - m_1} = J_{m_2} \cdot J_{m_1} = J_{m_2} \cdot J_{Q_x} \cdot J_{Q_y} \cdot J_{m_1} = J_{m_2} \begin{bmatrix} 1 & 0 \\ 0 & i \end{bmatrix} \begin{bmatrix} 1 & 0 \\ 0 & -i \end{bmatrix} J_{m_1}, \tag{7}$$

$$J_{m_2 + m_1} = J_{m_2} \cdot J_{H_x} \cdot J_{m_1} = J_{m_2} \cdot J_{Q_x} \cdot J_{Q_x} \cdot J_{m_1} = J_{m_2} \begin{bmatrix} 1 & 0 \\ 0 & i \end{bmatrix} \begin{bmatrix} 1 & 0 \\ 0 & i \end{bmatrix} J_{m_1}, \tag{8}$$

where Q_x and Q_y represent the fast axis of the QWP along the x axis and y axis directions respectively. Thus, by manipulating the orientations of two QWPs, the addition and subtraction of orders of VWPs can be achieved.

When the VWP is inserted into the laser cavity, an HWP, combined with a VWP, should be applied for achieving the self-reproduction of the mode after each round trip. So, when a horizontal polarized beam, represented by $E_1 = [0,1]^T$, passes through the HWP and VWP (as shown in Fig. 1), the Jones vector can be expressed as

$$E_2 = J_{\mathrm{VWP}} \cdot J_{\mathrm{HWP}} \cdot E_1 = \begin{bmatrix} \cos(m\varphi - 2\alpha) \\ \sin(m\varphi - 2\alpha) \end{bmatrix}. \tag{9}$$

It shows that the output is the mth-order CVB and by rotating the angle of α, arbitrary CVB on the equator of the higher-order Poincaré sphere can be generated.

In a round trip inside the cavity, the light E_1 passes through the HWP and VWP twice, which can be expressed as

$$E_3 = J_R \cdot J_{\mathrm{VWP}}(-\theta) \cdot J_{\mathrm{HWP}}(-\alpha) \cdot J_R \cdot E_2 = E_1, \tag{10}$$

where J_R represents the Jones matrix of the output coupling mirror. Then, the self-reproduction condition can be obtained.

Moreover, the output of order-switchable CVBs in the laser cavity can be realized by applying the OSVWP instead of the VWP, which provides a theoretical basis for the controlled

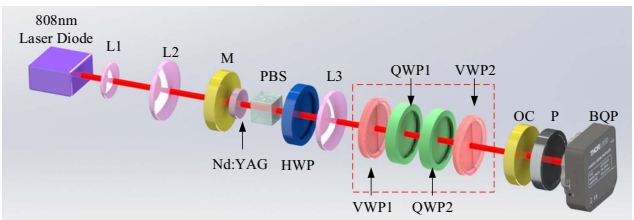

Fig. 1. Solid-state laser for the generation of mode-switchable high-order CVB. L1, collimating lens; L2, L3, focus lenses; M, input mirror (HT@808 nm, HR@1064 nm); Nd:YAG, laser crystal; PBS, polarizing beam splitter; HWP, half-wave plate; VWP1 & VWP2: vortex wave plates; QWP1 & QWP2: quarter-wave plates; OC, output coupling mirror; P, polarizer; BQP, beam quality profiler.

generation of order-switchable higher-order CVBs in a solid-state laser.

3. Experimental Setup

As shown in Fig. 1, the experimental device is kept at room temperature. A continuous-wave (CW) 808 nm-wavelength fiber-coupled laser diode (LD) serves as the pump source. The Nd:YAG crystal is used as the gain medium, with a length of 1.8 mm and a diameter of 10 mm. The surface of the crystal is coated with 808 nm and 1064 nm high antireflective films, whose transmittance is about 99.8%. The pump beam from the LD is focused to the center of the Nd:YAG crystal by a coupling lens bank, consisting of two convex lenses (L1 and L2) to maximize energy conversion efficiency. The focusing radius of the beam is about 300 μm.

Due to the long cavity length, the loss and threshold will increase. So, a convex lens, L3, with focal length $f = 150$ mm is inserted to solve the problem, which divides the resonator into two parts, L_A and L_B. $L_A = 12$ cm is the distance from the input mirror (M) to the lens (L3) and $L_B = 10$ cm is the distance from the lens (L3) to the output coupling mirror (OC). Antireflective films of 808 and 1064 nm are plated on the end face of the lens (L3), whose transmittance is about 99.8%. The input mirror (M) of the cavity is a plane mirror with high transmittance (HT) (99.8%) for 808 nm and high reflectivity (HR) (99.8%) for 1064 nm. A polarization beam splitter (PBS) in the laser cavity is utilized as the linearly polarization controller. Then, an HWP is inserted and mounted on a precision rotating bracket, which can accurately control the orientation of the linearly polarization beam incident on the VWP. A group of VWPs with two QWPs in adjacent VWPs are used as an OSVWP. A plane–concave lens is adopted as OC mirror for 1064 nm with transmittance of 10% and curvature of 1 m.

In order to clarify the modes of self-reproduction and polarization conversion in the cavity, an example is given in Fig. 2 by applying two VWPs of order $m = 1$. Two QWPs are placed between the VWPs. On the one hand, by rotating the angle of two QWPs, the addition and subtraction of the order of VWPs can be achieved. On the other hand, all the CVBs on the equator of the Poincaré sphere also can be manipulated by rotating the angle of the HWP[38]. When the fast-axis angles of QWP1 and QWP2 are rotated to the x-axis direction, the ultimate second-order CVB can be obtained.

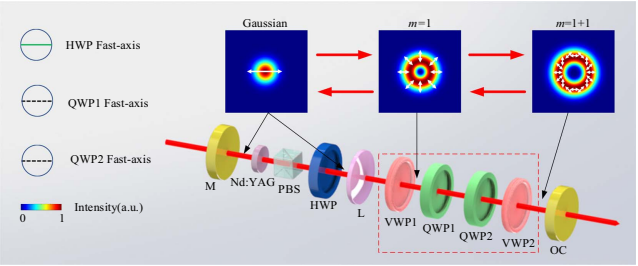

Fig. 2. Profile and polarization states of a tunable high-order CVB generated by a microchip laser which goes through a round-trip path in the cavity. M, input mirror; PBS, polarizing beam splitter; HWP, half-wave plate; VWP1&VWP2, q-plates of order m = 1; QWP1 and QWP2, quarter-wave plates; OC, output coupling mirror.

4. Results and Discussion

First, in the case of inserting two VWPs of order $m = 1$ into the cavity, rotating the fast-axis angle of HWP to 0, $\pi/8$, $\pi/4$, and $3\pi/8$, typical second-order CVBs of $\Phi = 0$, $\pi/4$, $\pi/2$, and $3\pi/4$ can be obtained, where Φ is coordinate system of the Poincaré sphere, also known as the polarization azimuth (PA). A beam quality profiler (THORLABS, BC106N-VIS/M) was used to measure the intensity distribution, as shown in Figs. 3(a1)–3(d1). Then, a polarizer, placed at angles of 0, $\pi/4$, and $\pi/2$, respectively, was used to monitor the polarization component of the output CVBs, as shown in Figs. 3(a2)–3(d4). At the same time, the Stokes vectors S_1, S_2, S_3 and PA of the second-order CVBs were measured using a polarizing camera (LUCID, PHX050S-QC) to confirm the polarization of the generated CVBs[14]. The Stokes vectors and PA distributions of the second-order CVBs of $\Phi = 0$, $\pi/4$, $\pi/2$, and $3\pi/4$ are shown in Fig. 4.

In addition, the experimental generation of the Gaussian beam and the second-order CVBs based on intracavity and extracavity methods are given in Fig. 5. Obviously, by rotating the angle of the HWP in the cavity, the second-order CVBs of $\Phi = 0$ and $\pi/2$ can also be generated. A polarizer was used to monitor the polarization distributions, the CVBs generated outside the cavity have an apparent diffraction ring, and the CVBs generated in the cavity have purer mode and better beam quality.

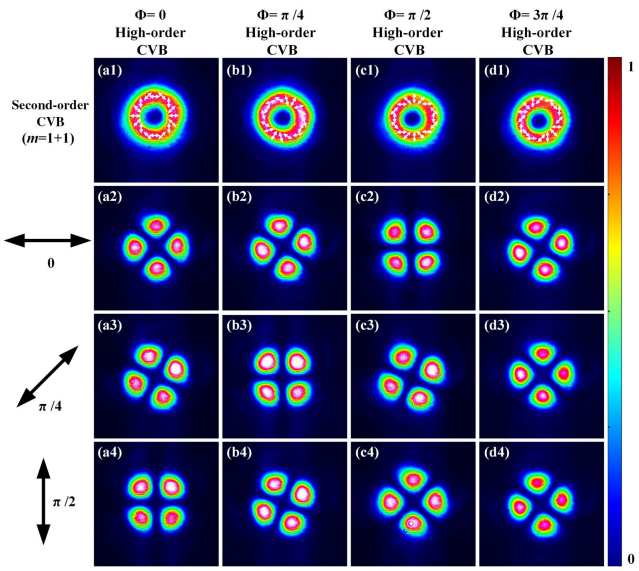

Fig. 3. (a1)–(d1) Intensity distributions of the second-order CVBs generated using the group of first-order VWPs and intensity distributions after passing through a linear polarizer oriented at different angles of (a2)–(d2) 0; (a3)–(d3) $\pi/4$; (a4)–(d4) $\pi/2$.

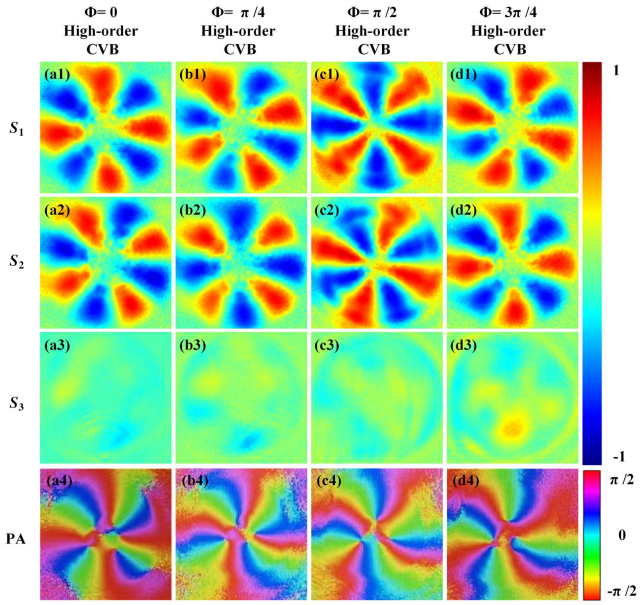

Fig. 4. Stokes parameters and polarization azimuth of the second-order CVBs. (a1)–(d1) S_1, (a2)–(d2) S_2, (a3)–(d3) S_3, (a4)–(d4) PA.

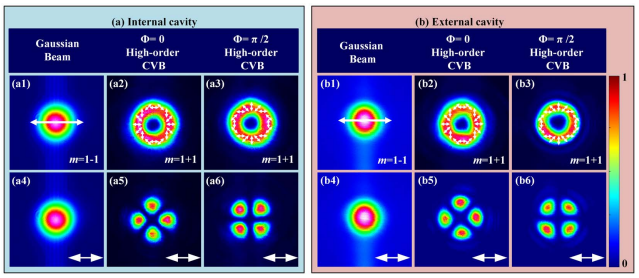

Fig. 5. Intensity distributions of the Gaussian beam and the second-order CVB are generated (a1)–(a3) in the cavity and (b1)–(b3) outside the cavity, respectively, using the group of first-order VWPs; intensity distributions after passing through the linear polarizer placed at 0 (a4)–(a6) inside and (b4)–(b6) outside the cavity.

The output spectrum measured by the spectrum analyzer (Yokogawa, AQ6370C) is shown in Fig. 6(a). An optical power meter (THORLABS, PM16-425) was utilized to measure laser power; the output power and pump power curves are shown in Fig. 6(b). The threshold power of TEM_{00} mode without VWP is about 0.3 W, with a slope efficiency of 15.1%. Because of the additional loss caused by the insertion of the VWP, the threshold for the laser TEM_{00} mode is about 1.5 W, and the corresponding slope efficiency is about 11.7%. When the pump power is increased to 4.8 W, TEM_{00} mode output power reaches 408 mW. However, the threshold of second-order CVBs is increased to 2.3 W. With the increase of pump power, the slope efficiency decreases gradually and stabilizes at 8.9%. We

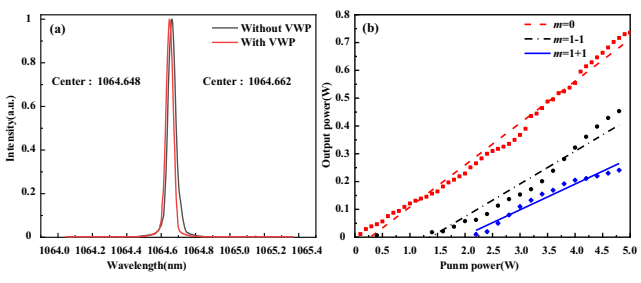

Fig. 6. (a) Output spectra. (b) Output power and pump power curves (the red is the Gaussian beam without VWP; the black and the blue are the Gaussian beam and second-order CVB with VWP).

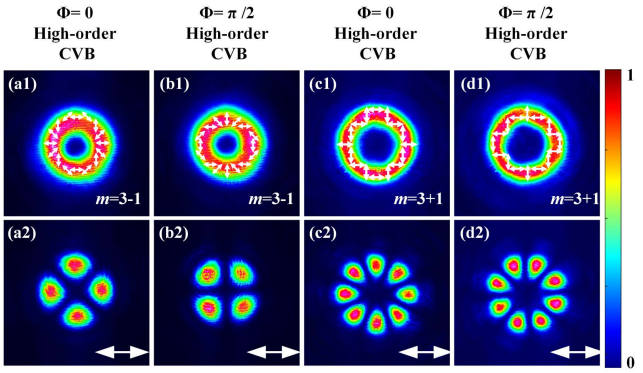

Fig. 7. (a1)–(d1) Intensity distributions of the second- and fourth-order CVBs are generated using the group of first- and third-order VWPs; (a2)–(d2) measured intensity distributions after passing through a linear polarizer oriented at 0.

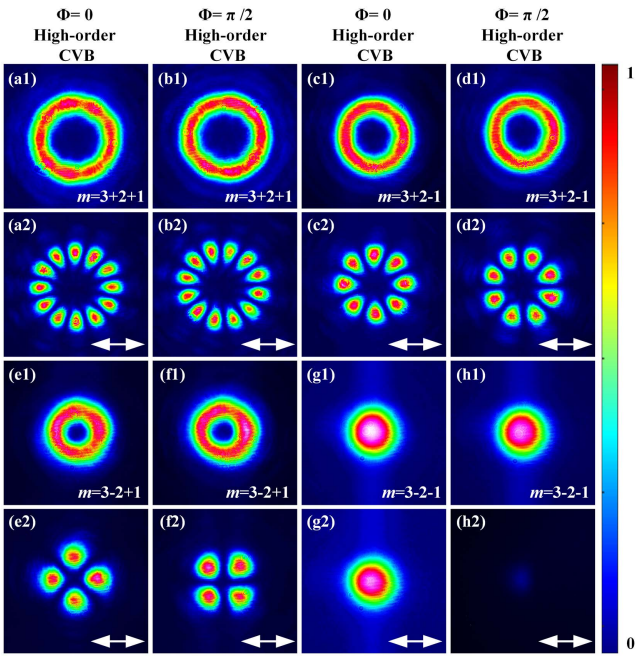

Fig. 8. (a1)–(h1) Intensity distributions of high-order CVBs are generated by different orders and numbers of VWP combinations inside the cavity; (a2)–(h2) measured intensity distributions after passing through a linear polarizer oriented at different angles of 0.

speculate that this is due to the thermal effect of the crystal with the increase of power. In addition, with the increase of beam order, the loss caused by the nonideal mode produced by the VWP also increases.

The combination of two different-order VWPs can still get the desired results. We changed the VWP combination of orders $m = 1$ and $m = 3$. The VWPs with smaller and larger orders were placed near the crystal, and the end of the OC mirror, separately. When the order of the CVB is larger, it will diverge faster. The second- and fourth- $(m = 3 \pm 1)$ order CVBs of $\Phi = 0$ and $\pi/2$ can be generated, as shown in Fig. 7. Then, the mode purity, the ratio of the minimum and maximum values (the CVBs pass through the linear polarizer at different angles), was measured by the optical power meter[39]. For the second- and fourth-order CVBs, the polarization purities are as high as 96.8% and 94.8%, and the sloping efficiencies are 4.45% and 3.06%, respectively. Furthermore, to achieve more order-switchable and higher-order CVBs, an OSVWP, consisting of three VWPs and four QWPs, was applied in the laser cavity. As shown in Fig. 8, with three VWPs of the first, second, and third order, the Gaussian beam, as well as the second-, fourth-, and sixth-order $(m = 3 \pm 2 \pm 1)$ CVBs of $\Phi = 0$ and $\pi/2$ are generated, which verifies that the mode-switchable CVBs between 2^{n-1} different orders can be generated by utilizing n pieces of VWPs.

5. Conclusion

In summary, we report and demonstrate a solid-state laser to obtain controlled generation of mode-switchable higher-order CVBs between different orders. A group of VWPs with two cascaded QWPs between the VWPs were utilized to achieve the mode conversion between TEM_{00} mode and CVBs, as well as the mode-switch of CVBs between different orders. Then, two first-order VWPs were used to generate a Gaussian beam and second-order CVBs with the slope efficiency of 11.7% and 8.9%, respectively. In addition, we obtained the second- and fourth-order CVBs with two VWPs of first and third order, of which the mode purities were as high as 96.8% and 94.8% and the sloping efficiencies were 4.45% and 3.06%, respectively. Furthermore, by applying three VWPs of first, second, and third orders, the mode-switchable higher-order CVBs among four different orders were generated, including a Gaussian beam and CVBs of second, fourth, and sixth order. By analogy, mode-switchable CVBs between 2^{n-1} different orders can be generated by utilizing n pieces of VWPs. The results have potential applications for the generation of ultrahigher-order CVBs, as well as mode-switchable higher-order CVBs between different orders.

Acknowledgement

This work was supported by the Postgraduate Research & Practice Innovation Program of Jiangsu Province (No. KYCX22_3813), the Jiangsu Province Key Research and Development Program (No. BE2022143), the National Natural Science Foundation of China (No. 62205133), and the Natural Science Foundation of Jiangsu Province (No. BK20190953).

References

1. Q. Zhan, "Cylindrical vector beams: from mathematical concepts to applications," Adv. Opt. Photonics **1**, 1 (2009).
2. S. Liu, S. Qi, Y. Zhang, P. Li, D. Wu, L. Han, and J. Zhao, "Highly efficient generation of arbitrary vector beams with tunable polarization, phase, and amplitude," Photonics Res. **6**, 228 (2018).
3. N. Daloi, P. Kumar, and T. N. Dey, "Guiding and polarization shaping of vector beams in anisotropic media," Phys. Rev. A **105**, 063714 (2022).
4. L. Rao, J. Pu, Z. Chen, and P. Yei, "Focus shaping of cylindrically polarized vortex beams by a high numerical-aperture lens," Opt. Laser Technol. **41**, 241 (2009).
5. M. Xian, Y. Xu, X. Ouyang, Y. Cao, S. Lan, and X. Li, "Segmented cylindrical vector beams for massively-encoded optical data storage," Sci. Bull. **65**, 2072 (2020).
6. Y. Liu, X. Ling, X. Yi, X. Zhou, H. Luo, and S. Wen, "Realization of polarization evolution on higher-order Poincaré sphere with metasurface," Appl. Phys. Lett. **104**, 191110 (2014).
7. Q. Song, A. Baroni, P. C. Wu, S. Chenot, V. Brandli, S. Vézian, B. Damilano, P. de Mierry, S. Khadir, and P. Ferrand, "Broadband decoupling of intensity and polarization with vectorial Fourier metasurfaces," Nat. Commun. **12**, 3631 (2021).
8. J. Wang, J. Yang, I. M. Fazal, N. Ahmed, Y. Yan, H. Huang, Y. Ren, Y. Yue, S. Dolinar, and M. Tur, "Terabit free-space data transmission employing orbital angular momentum multiplexing," Nat. Photonics **6**, 488 (2012).
9. R. Fickler, R. Lapkiewicz, W. N. Plick, M. Krenn, C. Schaeff, S. Ramelow, and A. Zeilinger, "Quantum entanglement of high angular momenta," Science **338**, 640 (2012).
10. Y. Kozawa, D. Matsunaga, and S. Sato, "Superresolution imaging via superoscillation focusing of a radially polarized beam," Optica **5**, 86 (2018).
11. Y. Zhang, M. Wang, Z. Ning, E. Cao, X. Liu, and Z. Nie, "Temporal effect on tight focusing, optical force and spin torque of high-order vector-vortex beams," Opt. Laser Technol. **149**, 107844 (2022).
12. S. Chen, Z. Xie, H. Ye, X. Wang, Z. Guo, Y. He, Y. Li, X. Yuan, and D. Fan, "Cylindrical vector beam multiplexer/demultiplexer using off-axis polarization control," Light Sci. Appl. **10**, 222 (2021).
13. Q. Zhao, S. Tu, Q. Lei, C. Guo, Q. Zhan, and Y. Cai, "Creation of cylindrical vector beams through highly anisotropic scattering media with a single scalar transmission matrix calibration," Photonics Res. **10**, 1617 (2022).
14. Z. Liu, Y. Liu, Y. Ke, Y. Liu, W. Shu, H. Luo, and S. Wen, "Generation of arbitrary vector vortex beams on hybrid-order Poincaré sphere," Photonics Res. **5**, 15 (2017).
15. S. Lou, Y. Zhou, Y. Yuan, T. Lin, F. Fan, X. Wang, H. Huang, and S. Wen, "Generation of arbitrary vector vortex beams on hybrid-order Poincaré sphere based on liquid crystal device," Opt. Express **27**, 8596 (2019).
16. R. Xu, P. Chen, J. Tang, W. Duan, S. Ge, L. Ma, R. Wu, W. Hu, and Y. Lu, "Perfect higher-order Poincaré sphere beams from digitalized geometric phases," Phys. Rev. Appl. **10**, 034061 (2018).
17. M. M. Sánchez-López, J. A. Davis, N. Hashimoto, I. Moreno, E. Hurtado, K. Badham, A. Tanabe, and S. W. Delaney, "Performance of a q-plate tunable retarder in reflection for the switchable generation of both first-and second-order vector beams," Opt. Lett. **41**, 13 (2016).
18. J. Jia, K. Zhang, G. Hu, M. Hu, T. Tong, Q. Mu, H. Gao, F. Li, C.-W. Qiu, and P. Zhang, "Arbitrary cylindrical vector beam generation enabled by polarization-selective Gouy phase shifter," Photonics Res. **9**, 1048 (2021).
19. D. Naidoo, F. S. Roux, A. Dudley, I. Litvin, B. Piccirillo, L. Marrucci, and A. Forbes, "Controlled generation of higher-order Poincaré sphere beams from a laser," Nat. Photonics **10**, 327 (2016).
20. S. Chen, X. Zhou, Y. Liu, X. Ling, H. Luo, and S. Wen, "Generation of arbitrary cylindrical vector beams on the higher order Poincaré sphere," Opt. Lett. **39**, 5274 (2014).
21. J. Hu, S. Kim, C. Schneider, S. Höfling, and H. Deng, "Direct generation of radially polarized vector vortex beam with an exciton-polariton laser," Phys. Rev. Appl. **14**, 044001 (2020).

22. J. Qi, W. Wang, B. Shi, H. Zhang, Y. Shen, H. Deng, W. Pu, X. Liu, H. Shan, and X. Ma, "Concise and efficient direct-view generation of arbitrary cylindrical vector beams by a vortex half-wave plate," Photonics Res. **9**, 803 (2021).
23. J. Qi, W. Yi, M. Fu, M. Zhu, J. Liu, G. Huang, J. Pan, S. Zhu, X. Chen, and W. Tabg, "Practical generation of arbitrary high-order cylindrical vector beams by cascading vortex half-wave plates," Opt. Express **29**, 25365 (2021).
24. W. Shu, X. Ling, X. Fu, Y. Liu, Y. Ke, and H. Luo, "Polarization evolution of vector beams generated by q-plates," Photonics Res. **5**, 64 (2017).
25. Q. Zhao, S. Tu, Q. Lei, C. Guo, Q. Zhan, and Y. Cai, "Creation of cylindrical vector beams through highly anisotropic scattering media with a single scalar transmission matrix calibration," Photonics Res. **10**, 1617 (2022).
26. R. Zhou, J. W. Haus, P. E. Powers, and Q. Zhan, "Vectorial fiber laser using intracavity axial birefringence," Opt. Express **18**, 10839 (2010).
27. R. Wang, S. He, S. Chen, J. Zhang, W. Shu, H. Luo, and S. Wen, "Electrically driven generation of arbitrary vector vortex beams on the hybrid-order Poincaré sphere," Opt. Lett. **43**, 3570 (2018).
28. J. Mendoza-Hernández, M. F. Ferrer-Garcia, J. A. Rojas-Santana, and D. Lopez-Mago, "Cylindrical vector beam generator using a two-element interferometer," Opt. Express **27**, 31810 (2019).
29. D. Chen, Y. Miao, H. Fu, H. He, J. Tong, and J. Dong, "High-order cylindrical vector beams with tunable topological charge up to 14 directly generated from a microchip laser with high beam quality and high efficiency," APL Photonics **4**, 106106 (2019).
30. D. Kim and J. Kim, "Direct generation of an optical vortex beam in a single-frequency Nd: YVO4 laser," Opt. Lett. **40**, 399 (2015).
31. D. Lin, J. Daniel, and W. Clarkson, "Controlling the handedness of directly excited Laguerre-Gaussian modes in a solid-state laser," Opt. Lett. **39**, 3903 (2014).
32. D. Wei, Y. Cheng, R. Ni, Y. Zhang, X. Hu, S. Zhu, and M. Xiao, "Generating controllable Laguerre-Gaussian laser modes through intracavity spin-orbital angular momentum conversion of light," Phys. Rev. Appl. **11**, 014038 (2019).
33. Y. Zhang, T. Wang, Y. Cheng, D. Wei, W. Yao, P. Chen, Y. Zhang, and M. Xiao, "Controllable laser output of high-quality cylindrical vector beam through intra-cavity mode conversion," Appl. Phys. Lett. **117**, 111105 (2020).
34. K. Huang, J. Zeng, J. Gan, Q. Hao, and H. Zeng, "Controlled generation of ultrafast vector vortex beams from a mode-locked fiber laser," Opt. Lett. **43**, 3933 (2018).
35. Y. Zhao, J. Fan, H. Shi, Y. Li, Y. Song, and M. Hu, "Intracavity cylindrical vector beam generation from all-PM Er-doped mode-locked fiber laser," Opt. Express **27**, 8808 (2019).
36. S. Ngcobo, I. Litvin, L. Burger, and A. Forbes, "A digital laser for on-demand laser modes," Nat. Commun. **4**, 1 (2013).
37. Z. Ma, W. Zhao, J. Zhao, J. Liu, Q. Jing, J. Dou, B. Li, and Y. Hu, "Generation of arbitrary higher-order Poincaré sphere beams from a ring fiber laser with cascaded Q-plates," Opt. Laser Technol. **156**, 108552 (2022).
38. X. Yi, Y. Liu, X. Ling, X. Zhou, Y. Ke, H. Luo, S. Wen, and D. Fan, "Hybrid-order Poincaré sphere," Phys. Rev. A **91**, 023801 (2015).
39. B. Sun, A. Wang, L. Xu, C. Gu, Y. Zhou, Z. Lin, H. Ming, and Q. Zhan, "Transverse mode switchable fiber laser through wavelength tuning," Opt. Lett. **38**, 667 (2013).